

High-Curie-temperature ferrimagnetism and ferroelectricity in $\text{Bi}_2\text{FeMoO}_6$

Peng Chen and Bang-Gui Liu*

*Beijing National Laboratory for Condensed Matter Physics,
Institute of Physics, Chinese Academy of Sciences, Beijing 100190, China*

(Dated: August 29, 2018)

BiFeO_3 is the most famous multiferroic material, but its G-type antiferromagnetism is highly desirable to be replaced by strong macroscopic magnetism beyond room temperature. Here we obtain double perovskite $\text{Bi}_2\text{FeMoO}_6$ with R3 (#146) space group by substituting Mo for 50% Fe in BiFeO_3 . Our first-principles calculated results show that it is a semiconductor with gap reaching to 0.725 eV, its net magnetic moment is $2\mu_B$ per formula unit, and its ferroelectric polarization is $85\mu\text{C}/\text{cm}^2$. This ferroelectricity is comparable with that of BiFeO_3 , but here the magnetism is a strong ferrimagnetism with Curie temperature of 650 K. Our first-principles phonon spectra establishes that this R3 phase is stable. Electric polarization and magnetic easy axis are shown to be in pseudo-cubic [111] axis. Our further analysis shows that the multiferroic mechanism is similar to that in BiFeO_3 . Therefore, this $\text{Bi}_2\text{FeMoO}_6$ can be used to achieve strong macroscopic magnetism and ferroelectricity well above room temperature, being useful for designing new multifunctional materials and devices.

PACS numbers: 75.85.+t, 75.30.-m, 77.80.-e, 75.10.-b

Multiferroic materials have great potentials to achieve new multifunctional devices for spintronics and data storage[1–5]. Recent years witnesses that perovskite BiFeO_3 becomes the most famous multiferroic material[4, 6–19]. It can show strong ferroelectricity with Curie temperature 1140K and antiferromagnetism with magnetic Neel temperature 640K[4, 8, 14]. In order to realize high-performance applications, one hopes to achieve strong macroscopic magnetism (ferromagnetism or ferrimagnetism) above room temperature instead of antiferromagnetism in the BiFeO_3 , keeping its strong ferroelectricity[4, 12–14]. For this purpose, it is a big step forward to predict and then synthesize multiferroic $\text{Bi}_2\text{FeCrO}_6$ whose double perovskite structure can be obtained from perovskite BiFeO_3 by substituting Cr for 50% Fe in the B site and forming alternate Fe and Cr ordering along the [111] axis[20–26]. However, it is difficult to keep the Fe and Cr ordering at a very high level because of the small difference between Fe and Cr[25, 26]. Therefore, it is highly desirable to realize much higher B-site ordering and achieve much better materials with strong macroscopic magnetism and ferroelectricity.

Here, we present a promising multiferroic $\text{Bi}_2\text{FeMoO}_6$ by substituting Mo for 50% Fe in perovskite BiFeO_3 and keeping alternate order of Fe and Mo along the [111] axis. It is a double perovskite phase with R3 (#146) space group. Considering that excellent Fe-Mo ordering has been achieved in double perovskite $\text{Sr}_2\text{FeMoO}_6$, a well-known half-metallic ferrimagnet[27–29], we believe that this substitution can lead to good ferrimagnetism because the moments at Fe and Mo sites cannot completely compensate any more. Our systematic first-principles calculations and structural analyses reveal that double perovskite $\text{Bi}_2\text{FeMoO}_6$ has a semiconductor gap of 0.725 eV and can show both strong ferroelectricity and strong ferrimagnetism with high Curie temperature. More detailed

results will be presented in the following.

Results

Structure optimization. Following Glazer's famous work on perovskite structures[30, 31], a systematic group analysis[32–34] reveals possible crystal structures for a specific double perovskite material with formula $A_2BB'O_6$. These group analyses can be used to simplify our structural optimizations. Here, we consider only those tilted BO_6 and $B'O_6$ octahedra allowed by group theory[34]. For optimizing $\text{Bi}_2\text{FeMoO}_6$, we start with a cubic perovskite structure with space group $\text{Fm}\bar{3}\text{m}$ (#225). This corresponds to $a^0a^0a^0$ in Glazer's notation. The optimization leads to rhombohedral lattice constant $a_c=5.558\text{\AA}$ and angle $\alpha_c=60^\circ$, primitive cell volume $V_c=121.41\text{\AA}^3$, and total energy $E_c=-67.3366\text{eV}$. In this structure, the O octahedra do not rotate around the [111] axis. Allowing the O octahedra to be able to rotate around the [111] axis, we can obtain an optimized structure with $\text{R}\bar{3}$ (#148) space group. It has rhombohedral lattice constant $a_1=5.644\text{\AA}$ and angle $\alpha_1=61.63^\circ$, primitive cell volume $V_1=131.76\text{\AA}^3$, and total energy $E_1=-69.5888\text{eV}$. Clearly, this symmetry breaking makes the total energy 2.2522 eV lower than the cubic phase. This structure still keeps inverse symmetry and therefore has no ferroelectricity, and in contrast with the cubic phase, the O octahedra of Fe and Mo do rotate by $+15.7^\circ$ and -17.4° around the [111] axis. This is a $a^-a^-a^-$ tilt (antiphase R_4^+ rotation) in Glazer's notation. For searching for the ground-state phase of $\text{Bi}_2\text{FeMoO}_6$, it is useful to compare it with BiFeO_3 [7, 14, 16, 17] and $\text{Bi}_2\text{FeCrO}_6$ [20–24] whose ground state phases are R3c (#161) and R3 (#146) phases, respectively. Because %50 Fe is substituted by Mo, there is no R3c structure for $\text{Bi}_2\text{FeMoO}_6$ and we should turn to the R3 structure for possible candidate of the ground-state phase of $\text{Bi}_2\text{FeMoO}_6$. For

this purpose, we allow the Fe ion to have a Γ_4^- displacement along the [111] direction[17, 35, 36]. This inverse symmetry breaking makes the total energy move further downward when we carefully optimize the structure. Consequently, we obtain a rhombohedral structure with space group R3 (#146). This optimized structure has rhombohedral lattice constant $a_2=5.743\text{\AA}$ and angle $\alpha_2=59.76^\circ$, primitive cell volume $V_2=133.24\text{\AA}^3$, and total energy $E_2=-69.8186\text{eV}$. This energy is 0.2298 and 2.4820 eV lower than the R $\bar{3}$ (#148) and Fm $\bar{3}m$ (#225), respectively. Considering its similarity with BiFeO₃ and Bi₂FeCrO₆, we believe that this R3 structure is the ground-state phase for Bi₂FeMoO₆. Our analysis results show that the tilting of oxygen octahedra of Fe and Mo can be described with rotation angles of $+17.8^\circ$ and -17.0° . It is clear that the three-fold rotational symmetry around the [111] axis is kept, but the calculated bond angles of Fe-O-Mo (150.0°), O-Fe-O (163.3°), and O-Mo-O (168.6°) deviate substantially from 180° . These reveal that the oxygen octahedra are substantially deformed. We illustrate the crystal structure and local octahedral tilting and deformation in Fig. 1 and summarize our calculated parameters in Table I. Although we have let only the Fe ion move along the [111] direction with respect to its oxygen environment in the initial structure, the optimization makes all the four cations coherently move along the [111] direction with respect to their oxygen environments, and we shall show that these coherent displacements are favorable to form ferroelectricity.

TABLE I: Main parameters of the fully optimized double perovskite Bi₂FeMoO₆ with the #146 space group: rhombohedral lattice constant (a) and angle (α), relative coordinates of the different ions, and rotational angles of the O octahedron of Fe ($\Delta\theta_{\text{Fe}}$) and Mo ($\Delta\theta_{\text{Mo}}$).

a	5.743 \AA	α	59.76 $^\circ$
Bi	0.2244	0.2244	0.2244
	0.7289	0.7289	0.7289
Fe	0.0000	0.0000	0.0000
Mo	0.5089	0.5089	0.5089
O	0.8432	0.6774	0.2913
	0.2913	0.8432	0.6774
	0.6774	0.2913	0.8432
	0.1765	0.3511	0.7917
	0.7917	0.1765	0.3511
	0.3511	0.7917	0.1765
$\Delta\theta_{\text{Fe}}$	17.8 $^\circ$	$\Delta\theta_{\text{Mo}}$	-17.0 $^\circ$

Magnetic moment and electronic energy gap. Presented in Fig. 2 is our GGA calculated spin-dependent density of states (DOS) and energy bands of the optimized double perovskite Bi₂FeMoO₆ (R3 phase). Our analysis indicates that in the spin-up channel, the three filled Fe t_{2g} bands merges into the oxygen p bands

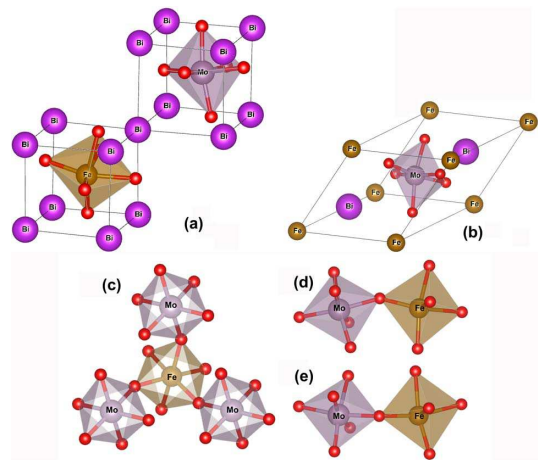


FIG. 1: (Color online.) Crystal structure (a,b) and local changes of O octahedra of Fe and Mo (c-e) of double perovskite Bi₂FeMoO₆ with the #146 space group. (a) A schematic crystal structure, showing the alternate occupation of Fe and Mo at the B-sites of the simple perovskite structure along the [111] direction. (b) The primitive cell of the double perovskite structure with the O octahedron of Mo shown. (c) The relative rotation projected on the (111) plane of an O octahedron of Fe with respect to three of the nearest O octahedra of Mo. (d) The two neighboring O octahedra of Fe and Mo projected on the plane of the Fe-O-Mo triangle, reflecting the Fe-O-Mo bond angle. (e) the same two O octahedra of Fe and Mo projected on the perpendicular plane including the Fe and Mo ions, showing local deformation.

and the two filled Fe eg bands are separated from them, and the empty bands, from Mo 4d states, are above 0.65 eV. It can be seen that there is a narrow semiconductor gap, 0.059 eV, which is formed between the three filled Mo 4d bands and the three empty Fe 3d ones in the spin-down channel. This narrow GGA gap remains open as long as the optimization is done with high force convergence standard of 1 meV/ \AA or smaller, or else it can become a pseudo-gap indicating a metallic electron phase[37]. Totally, we have five Fe d electrons in the spin-up channel and three Mo d electrons in the spin-down channel, and thus the magnetic moment per formula unit is equivalent to $2\mu_B$, which is consistent with the calculated data. The small gap value is due to the well-known under-estimation of GGA on semiconductor gaps. In order to make an accurate calculation of the semiconductor gap, we use a modified Becke-Johnson (mBJ) exchange functional to replace the GGA one. Our mBJ calculated gap, 0.725 eV, should be a much better value for the true gap because mBJ has been proved to give accurate semiconductor gaps for most of semiconductors. We also use other exchange-correlation schemes to calculate the semiconductor gap and conclude that there is certainly a finite semiconductor gap for the double perovskite Bi₂FeMoO₆.

Ionic displacements towards ferroelectricity. In Fig. 3 we shows the relative distances between the

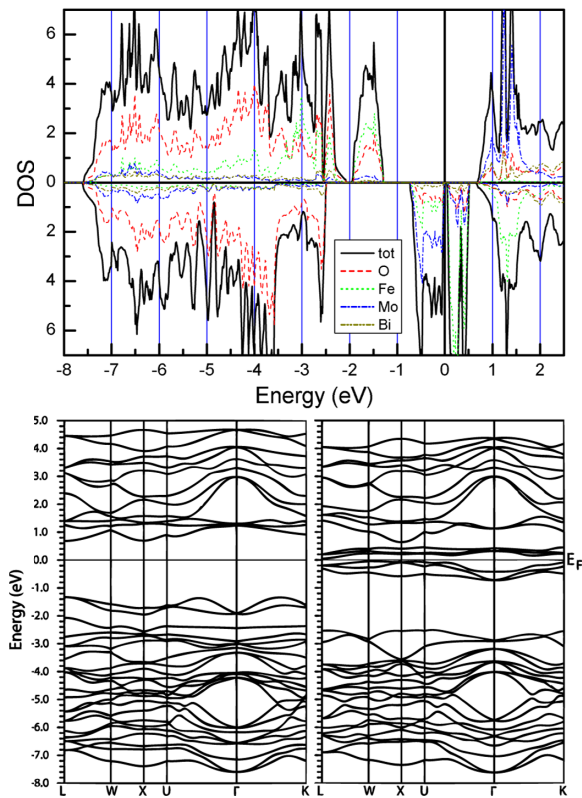


FIG. 2: Electronic structure of the double perovskite $\text{Bi}_2\text{FeMoO}_6$ calculated with GGA. Upper: the spin-resolved density of states (DOS, state/eV per primitive cell), in which the upper part are spin-up DOS and the lower part spin-down DOS. Lower: the spin-resolved energy band structures, in which the left part shows spin-up bands and the lower part spin-down ones.

cations and their nearest O environment along the [111] direction for the three structures: #225, #148, and #146. The vertical line, Δ_1 - Δ_4 , indicates the position of three O atoms forming a regular triangle perpendicular to the [111] axis. The O-O bond lengths and rotation angles of the O octahedron are presented at the top of vertical lines. The lengths of the primitive cells along [111] direction are given at the right-most sides of the [111] lines. Comparing the #148 structure with the #225, Fe and Mo are still at the centers of their O octahedra, respectively, and the local asymmetry at Bi1 and Bi2 ions in the #148 structure becomes much larger than in the latter. However, the displacements of Bi1 and Bi2 with respect to their O environments are opposite to each other along the [111] axis, which means that there is still no ferroelectricity, but a Bi-induced antiferroelectricity, in the #148 structure. In contrast, the #146 structure is very different in that all its cations have in-phase displacements in the same [111] direction with respect to their O environment. In order to get a clearer insight, we further investigate the displacements of cations with respect to their O environments along the [111] direction

in terms of two cation-related quantities, Plus and Minus. The Plus (Minus) value of a cation is defined as the summation (subtraction) of the two distances from the cation to its left O triangle and right triangle along the [111] axis. The Plus value indicates the distance between the two O triangles on the two sides of the cation, and the Minus value describes the displacement of the cation with respect to its two O triangles along the [111] direction. We present the Plus and Minus values of the four cations in the #146 phase of the $\text{Bi}_2\text{FeMoO}_6$ in Table II. The Minus values of all the four cations are negative and thus in-phase, and therefore indicate ferroelectricity in the $\text{Bi}_2\text{FeMoO}_6$, being the same as those of the $\text{Bi}_2\text{FeCrO}_6$ which has a strong ferroelectricity along the [111] direction[20–25, 38].

Electron density distributions implying ferroelectricity. We present in Fig. 4 the electron density distributions in a typical plane for the #148 and #146 structures of the $\text{Bi}_2\text{FeMoO}_6$. The plane, namely A plane, is defined to include the Fe-Bi-Mo-Bi line along the [111] axis and the two nearest O atoms on the two sides of the Mo atom. The charge and spin density distributions can be compared between the two structures. An asymmetry can be seen near the two Bi atoms for the charge density distribution between -8 and 0 eV for the two structures, and it is, however, in phase for the #146 structure but out of phase for the other. Furthermore, we can easily see an in-phase asymmetry in the Bi 6s charge density distribution in the #146 structure, but cannot in the other. As for the spin density distribution, a difference can also be found between the two Bi atoms for the #146 structure. These electron density properties are consistent with the in-phase displacements of the cations in the [111] direction.

DFT calculations of ferroelectric polarization. Finally, we quantitatively investigate the ferroelectricity of the $\text{Bi}_2\text{FeMoO}_6$ through modern DFT-based calculations[39]. Since the R3 (#148) as the reference structure has no semiconductor gap under GGA, we make quantitative calculations of the electric polarization by using GGA+U[40, 41] and HSE06[42, 43] methods which have been implemented in VASP package. For the GGA+U scheme, we use three sets of (U, J) parameters for Fe, keeping the same (U, J)=(2.5eV, 0.5eV) for Mo. With these schemes and parameters, the semiconductor gaps range from 0.23 to 0.91 eV, but it should be kept in mind that accurate semiconductor gap needs to be calculated with mBJ scheme. We summarize the calculational parameters and electric polarization results in Table II. These results mean that the $\text{Bi}_2\text{FeMoO}_6$ (#146) has a large spontaneous ferroelectric polarization $85\mu\text{C}/\text{cm}^2$, which is almost independent of calculational schemes and parameters. Therefore the $\text{Bi}_2\text{FeMoO}_6$ is an excellent ferroelectric material.

Ferroelectric switching and phonon spectra. It should be pointed out that the R3 (#146) phase is de-

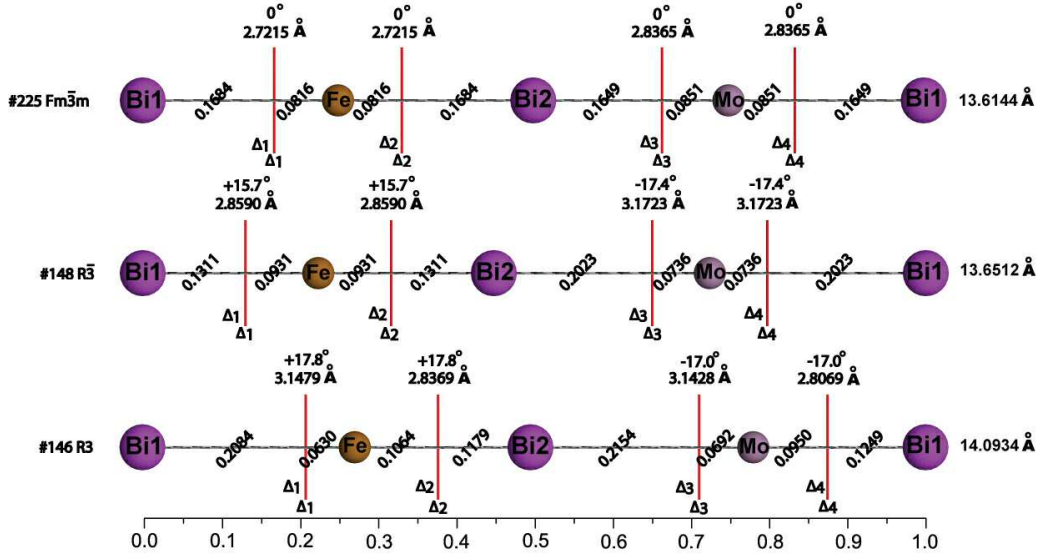


FIG. 3: (Color online.) The relative distances (tilted numbers) between the positive ions (Bi1, Fe, Bi2, Mo) and the centers of the nearest O triangles (Δ_1 , Δ_2 , Δ_3 , Δ_4) and the relative rotational angles of the O triangles around the $[111]$ axis, compared among the three crystal structures with the space groups: #225, #148, and #146. The values in \AA above the O triangles are their edge lengths (O-O distances), respectively. The three values at the rightmost side are the lengths of the primitive cells along the $[111]$ direction. Notice: there is a rotational angle of 60° between Δ_1 and Δ_2 , and between Δ_3 and Δ_4 .

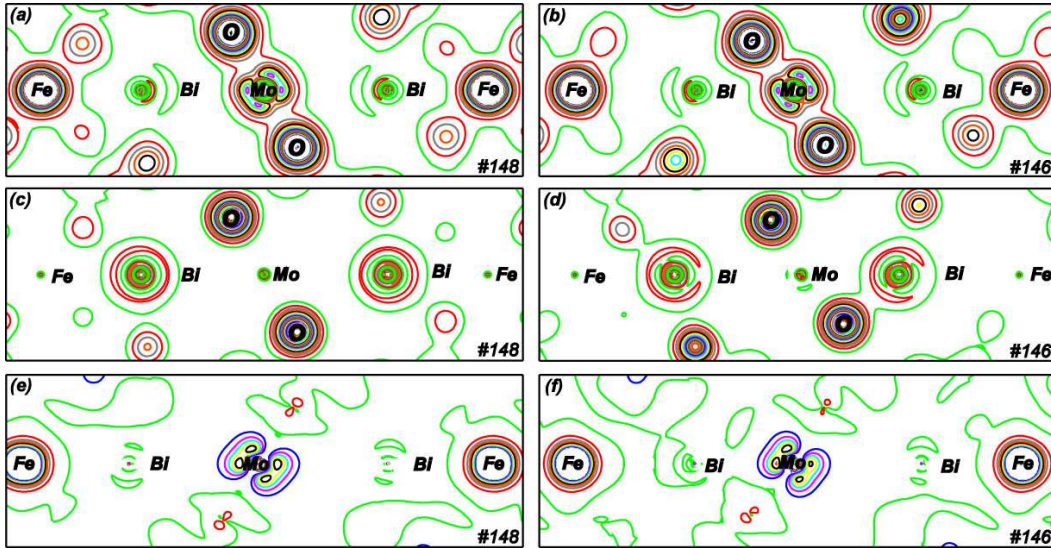


FIG. 4: (Color online.) The electron density distributions in the A plane of the double perovskite $\text{Bi}_2\text{FeMoO}_6$ with the #148 [left: (a), (c), (e)] and #146 [right: (b), (d), (f)] space groups in comparison. (a) and (b) show the charge density distributions of the valence electrons between -8 and 0 eV, ranging from 0 to $3|e|/\text{\AA}^3$ with a contour increment of $0.15|e|/\text{\AA}^3$; (c) and (d) the charge density distribution of Bi 6s and O 2s electrons between -21 and -9 eV, ranging from 0 to $2|e|/\text{\AA}^3$ with a contour increment of $0.1|e|/\text{\AA}^3$; and (e) and (f) the spin density distributions of the valence electrons between -8 and 0 eV, ranging from 0 to $2\mu_B/\text{\AA}^3$ with a contour increment of $0.1\mu_B/\text{\AA}^3$.

generate in total energy. For example, one of them, with the polarization P , can be changed into another one with the polarization $-P$. Using a linear interpolation method and performing full optimization on the basis of the two with $\pm P$, we can obtain a reversal path connecting them, with the $R\bar{3}$ (#148) phase naturally appearing as an in-

termediate structure. The calculated energy curve along the path[44, 45] is shown in Fig. 5(a). Most importantly, we have performed first-principles calculations on phonon spectra for these two phases. The calculated phonon spectra are presented in Fig. 5 (b) and (c). These results show that both of them are dynamically stable, in

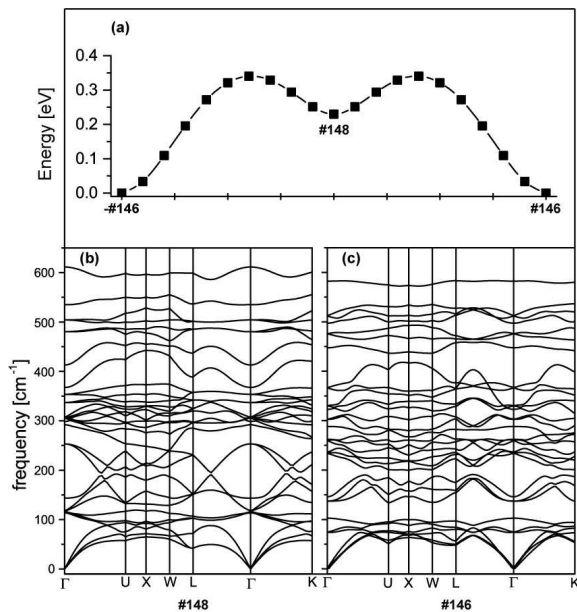


FIG. 5: (Color online.) Polarization reversal path (a) and structural stability (b,c). (a) A reversal path of the ferroelectric phase of #146 through the intermediate phase of #148. (b) Phonon spectra of the intermediate phase (#148). (c) Phonon spectra of the ferroelectric phase (#146).

addition to the static stability of the R3 phase in terms of formation heat calculations[37].

Robust multiferroicity. All our above analyses of the ion displacements and electronic density distributions indicate that the double perovskite $\text{Bi}_2\text{FeMoO}_6$ in the #146 structure should have a strong ferroelectricity in the pseudocubic [111] direction. More importantly, our DFT-based Berry phase calculation establishes that it indeed has strong ferroelectricity P along the direction. Its electric polarization, reaching to $85\mu\text{C}/\text{cm}^2$, is comparable with that of the BiFeO_3 , which indicates that it should have a high ferroelectric Curie temperature. In addition, our analysis indicate that there is another degenerate ground-state phase with ferroelectricity $-P$, which implies that the polarization can be reversed through the #148 structure as an intermediate structure in between. On the other hand, we also calculate spin exchange energies and Curie temperatures for the multiferroic phase and the intermediate one. The simulated curves for magnetization and susceptibility are presented in Fig. 6 (a) and (b), indicating a high magnetic Curie temperature of 650 K[37]. Our magnetocrystalline calculations including the spin-orbit coupling are presented in Fig. 6(c). The curve for the #146 phase can be fitted with $E = E_0 + E_{\text{MA}} \sin^2(\frac{\pi}{180}\omega)$, with $E_{\text{MA}} = 1.52 \pm 0.005$ meV. This indicates that the easy axis is the pseudocubic [111] and the magneto-crystalline anisotropic energy is 1.52 meV. It is interesting that the #148 phase also has ferrimagnetic order with a net magnetic moment of 2

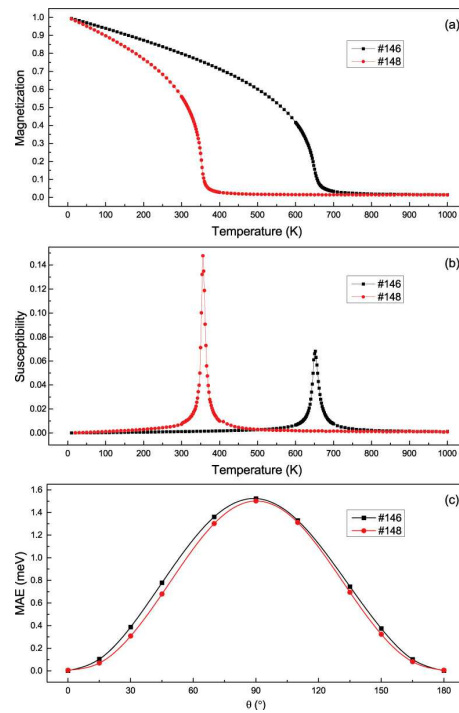


FIG. 6: (Color online.) The magnetism of the ferroelectric phase and the intermediate phase of the double perovskite $\text{Bi}_2\text{FeMoO}_6$. Monte Carlo simulated results for magnetization (a) and susceptibility (b) of the two phases. (c) The magnetocrystalline energies of the two phases, defined as a functions of the polar angle (in degree) from the [111] direction.

μ_B below 360 K and magnetocrystalline energy 1.50 meV with the easy axis long the [111]. For convenience, we also summarize the key multiferroic parameters in Table II. Therefore, it has been established that the double perovskite $\text{Bi}_2\text{FeMoO}_6$ is a robust multiferroic material with high Curie temperatures.

Discussion

We have shown robust ferrimagnetism and ferroelectricity in the double perovskite $\text{Bi}_2\text{FeMoO}_6$ in the R3 (#146) structure. The large ferroelectric polarization in Table II means that this $\text{Bi}_2\text{FeMoO}_6$ is comparable with the BiFeO_3 in ferroelectricity, and in addition the strong ferrimagnetism is shown to be able to persist at high temperature far beyond room temperature. Because the $\text{Bi}_2\text{FeMoO}_6$ is stable in terms of both static and dynamical calculations, it could be synthesized soon. When realized experimentally, it should be a promising multiferroic material, especially for spintronics applications. Because of its robust multiferroic properties, the $\text{Bi}_2\text{FeMoO}_6$ can be used to form some interesting composite structures such as multiferroic superlattices[46].

As for the mechanism of multiferroicity, it is similar to that of the BiFeO_3 , except that here the Mo moment cannot be completely compensated by the Fe mo-

TABLE II: Calculated Plus and Minus values (\AA) of cations, DFT-calculated ferroelectric polarizations, and summarized key multiferroic parameters of the double perovskite $\text{Bi}_2\text{FeMoO}_6$.

Ionic displacement analysis				
	Bi1	Fe	Bi2	Mo
Plus	4.7337	2.3836	4.6978	2.3142
Minus	-1.1771	-0.6164	-1.3736	-0.3646
Berry phase calculations of polarization				
scheme	Fe(U,J) / Mo(U,J) (eV)			P ($\mu\text{C}/\text{cm}^2$)
GGA+U	(2.0,0.8) / (2.5,0.5)			85.4
	(4.0,0.8) / (2.5,0.5)			85.5
	(8.0,0.8) / (2.5,0.5)			84.7
HSE06	-			85.4
Key multiferroic parameters				
Ferrimagnetism	M	$2 \mu_B$	T_c	650 K
Ferroelectricity	P	$85 \mu\text{C}/\text{cm}^2$	T_c	high

ment, producing the finite net magnetic moment $2\mu_B$ per formula unit. It is interesting that the ferrimagnetic Curie temperature is predicted to be also similar to the Neel temperature of the BiFeO_3 . The ferri-distortive rotations of the oxygen octahedra of Fe and Mo is favorable to stabilize the Bi-dominated antiferroelectricity in the #148 structure of the $\text{Bi}_2\text{FeMoO}_6$. These ferri-distortive rotations of the O octahedra of Fe and Mo are similar to antiferrodistortive rotations of O octahedra of Fe in the BiFeO_3 [35]. It is also clear that these ferri-distortive rotations coexist with the ferroelectricity in the #146 phase. It should be pointed out that in addition to the the multiferroic #146 phase, there should exist some metastable phases for $\text{Bi}_2\text{FeMoO}_6$, with the #148 structure being one of them. This is also similar to BiFeO_3 for which many metastable structures have been found[14, 17–19, 36].

In summary, we have investigated double perovskite $\text{Bi}_2\text{FeMoO}_6$ through systematic DFT calculations and structural analyses. Our careful GGA optimization reveals that the $\text{Bi}_2\text{FeMoO}_6$ in the #146 structure is a ferrimagnetic semiconductor. The net moment reaches to $2\mu_B$ per formula unit because the magnetic moments of Fe and Mo cannot be canceled, and the semiconductor gap corrected with mBJ potential reaches to 0.725 eV. The O octahedra of Fe and Mo ions have rotation angles of $+17.8^\circ$ and -17.0° around the [111] axis, respectively. Our analyses of the electronic structure and ionic displacements indicate strong ferroelectricity in the $\text{Bi}_2\text{FeMoO}_6$. Our DFT-based electric polarization calculations directly shows that the $\text{Bi}_2\text{FeMoO}_6$ has strong ferroelectricity in the [111] direction. Our first-principles phonon spectra show that this multiferroic phase is stable. Therefore, it has been established that

the $\text{Bi}_2\text{FeMoO}_6$ is a promising multiferroic material with strong ferroelectricity and high ferrimagnetic Curie temperature far beyond room temperature. With the spin-orbit effect into account, our calculation show that the magnetic easy axis is also in the [111] axis. The magnetocrystalline anisotropy should be manipulated as has been done in $\text{Sr}_2\text{FeMoO}_6$ film materials[29]. This multiferroic material can be useful for designing new multifunctional materials and devices in the future.

Methods

We use projector augmented-wave (PAW)[47] plus pseudo-potential methods within the density functional theory[48, 49], as implemented in the Vienna ab initio simulation package (VASP) [44, 45], to optimize the crystal structures and then study the electronic structures, ferroelectricity, and magnetic properties. The spin-polarized generalized-gradient approximation (GGA)[50], to the electronic exchange-correlation functional, is used to do structure optimization. We use a plane wave basis set with a maximum kinetic energy of 500 eV and a $12 \times 12 \times 12$ k-point mesh generated with the Monkhorst-Pack scheme[51]. During optimization, all of the structures were fully relaxed until the largest force between the atoms become less than $1 \text{ meV}/\text{\AA}$.

Phonon spectra are calculated with first-principles perturbation method with norm-conserving pseudo-potentials as implemented in package Quantum-ESPRESSO [52]. The magnetic anisotropy energy (MAE) due to the spin-orbit coupling is determined by the force theorem, and calculated in terms of the total energy with respect to the [111] direction. We use a modified Becke-Johnson exchange potential to accurately calculate semiconductor gaps[53]. We use modern Berry phase method[39] and take both GGA+U [40, 41] and HSE06 [42, 43] schemes to calculate electric polarization. For calculating magnetic Curie temperatures, we first construct an effective Heisenberg spin model through comparing total energies of the ferrimagnetic phase and other magnetic structures concerned[37], and then do standard Monte Carlo simulations in terms of the model.

* Corresponding author: bgliu@iphy.ac.cn

- [1] Wolf, S. A. *et al.* Spintronics: A spin-based electronics vision for the future. *Science* **294**, 1488-1495 (2001).
- [2] Dawber, M., Rabe, K. M. & Scott, J. F. Physics of thin-film ferroelectric oxides. *Rev. Mod. Phys.* **77**, 1083 (2005).
- [3] Rabe, K. M., Ahn, C. H., Triscone, J.-M. (Eds.), *Physics of Ferroelectrics - A Modern Perspective*, Springer-Verlag Berlin 2007.
- [4] Catalan, G. & Scott, J. F. Physics and applications of bismuth ferrite. *Adv. Mater.* **21**, 2463-2485 (2009).
- [5] Picozzi, S. & Ederer, C. First principles studies of multi-

- ferroic materials. *J. Phys.: Condens. Matter* **21**, 303201 (2009).
- [6] Bhide, V. G. & Multani, M. S. Mössbauer effect in ferroelectric-antiferromagnetic BiFeO₃. *Solid State Commun.* **3**, 271-274 (1965).
- [7] Moreau, J. M., Michel, C., Gerson, R. & James, W. J. Ferroelectric BiFeO₃ X-ray and neutron diffraction study. *J. Phys. Chem. Solids* **32**, 1315-1320 (1971).
- [8] Wang, J. *et al.* Epitaxial BiFeO₃ multiferroic thin film heterostructures. *Science* **299**, 1719-1722 (2003).
- [9] Nelson, C. T. *et al.* Domain dynamics during ferroelectric switching. *Science* **334**, 968-971 (2011).
- [10] Ramazanoglu, M. *et al.* Local weak ferromagnetism in single-crystalline ferroelectric BiFeO₃. *Phys. Rev. Lett.* **107**, 207206 (2011).
- [11] Infante, I. C. *et al.* Multiferroic phase transition near room temperature in BiFeO₃ films. *Phys. Rev. Lett.* **107**, 237601 (2011).
- [12] Scott, J. F. DATA STORAGE: Multiferroic memories. *Nature Mater.* **6**, 256-257 (2007).
- [13] Choi, T., Lee, S., Choi, Y. J., Kiryukhin, V. & Cheong, S.-W. Switchable ferroelectric diode and photovoltaic effect in BiFeO₃. *Science* **324**, 63-66 (2009).
- [14] Park, J.-G., Le, M. D., Jeong, J. & Lee, S. Structure and spin dynamics of multiferroic BiFeO₃. arXiv: 1409.0301.
- [15] Ederer, C. & Spaldin, N. A. Weak ferromagnetism and magnetoelectric coupling in bismuth ferrite. *Phys. Rev. B* **71**, 060401(R) (2005).
- [16] Neaton, J. B., Ederer, C., Waghmare, U. V., Spaldin, N. A. & Rabe, K. M. First-principles study of spontaneous polarization in multiferroic BiFeO₃. *Phys. Rev. B* **71**, 014113 (2005).
- [17] Ravindran, P., Vidya, R., Kjekshus, A., Fjellvag, H. & Eriksson, O. Theoretical investigation of magnetoelectric behavior in BiFeO₃. *Phys. Rev. B* **74**, 224412 (2006).
- [18] Dupe, B., Prosandeev, S., Geneste, G., Dkhil, B. & Bellaiche, L. BiFeO₃ Films under tensile epitaxial strain from first principles. *Phys. Rev. Lett.* **106**, 237601 (2011).
- [19] Yang, Y., Ren, W., Stengel, M., Yan, X. H. & Bellaiche, L. Revisiting properties of ferroelectric and multiferroic thin films under tensile strain from first principles. *Phys. Rev. Lett.* **109**, 057602 (2012).
- [20] Baettig, P. & Spaldin, N. A. Ab initio prediction of a multiferroic with large polarization and magnetization. *Appl. Phys. Lett.* **86**, 012505 (2005).
- [21] Baettig, P., Ederer, C. & Spaldin, N. A. First principles study of the multiferroics BiFeO₃, Bi₂FeCrO₆, and BiCrO₃: Structure, polarization, and magnetic ordering temperature. *Phys. Rev. B* **72**, 214105 (2005).
- [22] Nechache, R. *et al.* Growth, structure, and properties of epitaxial thin films of first-principles predicted multiferroic Bi₂FeCrO₆. *Appl. Phys. Lett.* **89**, 102902 (2006).
- [23] Kamba, S. *et al.* Infrared and magnetic characterization of multiferroic Bi₂FeCrO₆ thin films over a broad temperature range. *Phys. Rev. B* **77**, 104111 (2008).
- [24] Aissa, B., Nechache, R., Therriault, D., Rosei, F. & Nedil, M. High-frequency electromagnetic properties of epitaxial Bi₂FeCrO₆ thin films grown by pulsed laser deposition. *Appl. Phys. Lett.* **99**, 183505 (2011); *Appl. Phys. Lett.* **99**, 239903 (2011).
- [25] Nechache, R., Harnagea, C. & Pignolet, A. Multiferroic properties-structure relationships in epitaxial Bi₂FeCrO₆ thin films: recent developments. *J. Phys.: Condens. Matter* **24**, 096001 (2012).
- [26] Nechache, R. & Rosei, F. Recent progress in nanostructured multiferroic Bi₂FeCrO₆ thin films. *J. Solid State Chem.* **189**, 13C20 (2012).
- [27] Hauser, A. J. *et al.* Unlocking the potential of half-metallic Sr₂FeMoO₆ films through controlled stoichiometry and double-perovskite ordering. *Phys. Rev. B* **83**, 014407 (2011).
- [28] Erten, O. *et al.* Theory of half-metallic ferrimagnetism in double perovskites. *Phys. Rev. Lett.* **107**, 257201 (2011).
- [29] Du, C. *et al.* Control of magnetocrystalline anisotropy by epitaxial strain in double perovskite Sr₂FeMoO₆ films. *Phys. Rev. Lett.* **110**, 147204 (2013).
- [30] Glazer, A. M. The classification of tilted octahedra in perovskites. *Acta Cryst. B* **28**, 3384-3392 (1972).
- [31] Glazer, A. M. Simple ways of determining perovskite structures. *Acta Cryst. A* **31**, 756-762 (1975).
- [32] Woodward, P. M. Octahedral tilting in perovskites. II. structure stabilizing forces. *Acta Cryst. B* **53**, 44-66 (1997).
- [33] Howard, C. J. & Stokes, H. T. Group-theoretical analysis of octahedral tilting in perovskites. *Acta Cryst. B* **54**, 782-789 (1998).
- [34] Howard, C. J., Kennedy, B. J. & Woodward, P. M. Ordered double perovskites - a group-theoretical analysis. *Acta Cryst. B* **59**, 463-471 (2003).
- [35] Dieguez, O., Aguado-Puente, P., Junquera, J. & Iniguez, J. Domain walls in a perovskite oxide with two primary structural order parameters: First-principles study of BiFeO₃. *Phys. Rev. B* **87**, 024102 (2013).
- [36] Dieguez, O., Gonzalez-Vazquez, O. E., Wojdel, J. C. & Iniguez, J. First-principles predictions of low-energy phases of multiferroic BiFeO₃. *Phys. Rev. B* **83**, 094105 (2011).
- [37] Li, S.-D., Chen, P. & Liu, B.-G. Promising ferrimagnetic double perovskite oxides towards high spin polarization at high temperature. *AIP Advances* **3**, 012107 (2013).
- [38] Song, Z.-W. & Liu, B.-G. Electronic structure and magnetic and optical properties of double perovskite Bi₂FeCrO₆ from first-principles investigation. *Chin. Phys. B* **22**, 047506 (2013).
- [39] King-Smith, R. D. & Vanderbilt, D. Theory of polarization of crystalline solids. *Phys. Rev. B* **47**, 1651(R) (1993).
- [40] Anisimov, V. I., Zaanen, J. & Andersen, O. K. Band theory and Mott insulators: Hubbard U instead of Stoner. *Phys. Rev. B* **44**, 943 (1991).
- [41] Anisimov, V. I., Aryasetiawan, F. & Lichtenstein, A. I. First-principles calculations of the electronic structure and spectra of strongly correlated systems: the LDA+U method. *J. Phys.: Condens. Matter* **9**, 767 (1997).
- [42] Heyd, J., Scuseria, G. E. & Ernzerhof, M. Hybrid functionals based on a screened Coulomb potential. *J. Chem. Phys.* **118**, 8207 (2003); **124**, 219906 (2006).
- [43] Heyd, J., Peralta, J. E., Scuseria, G. E. & Martin, R. L. Energy band gaps and lattice parameters evaluated with the Heyd-Scuseria- Ernzerhof screened hybrid functional. *J. Chem. Phys.* **123**, 174101 (2005).
- [44] Kresse, G. & Hafner, J. Ab initio molecular dynamics for liquid metals. *J. Phys. Rev. B* **47**, 558(R) (1993).
- [45] Kresse, G. & Furthmüller, J. Efficient iterative schemes for ab initio total-energy calculations using a plane-wave basis set. *Phys. Rev. B* **54**, 11169 (1996).
- [46] Song, G. & Zhang, W.-Y. First-principles study on the phase diagram and multiferroic properties of

- (SrCoO₃)₁/(SrTiO₃)₁ superlattices. *Sci. Rep.* **4**, 4564 (2014).
- [47] Blochl, P. E. Projector augmented-wave method. *Phys. Rev. B* **50**, 17953 (1994).
- [48] Hohenberg, P. & Kohn, W. Inhomogeneous electron gas. *Phys. Rev.* **136**, B864 (1964).
- [49] Kohn, W. & Sham, L. Self-consistent equations including exchange and correlation effects. *J. Phys. Rev.* **140**, A1133 (1965).
- [50] Perdew, J. P., Burke, K. & Ernzerhof, M. Generalized gradient approximation made simple. *Phys. Rev. Lett.* **77**, 3865 (1996).
- [51] Monkhorst, H. J. & Pack, J. D. Special points for Brillouin-zone integrations. *Phys. Rev. B* **13**, 5188 (1976).
- [52] Giannozzi, P. *et al.* QUANTUM ESPRESSO: a modular and open-source software project for quantum simulations of materials. *J. Phys.: Condens. Matter* **21**, 395502 (2009) .
- [53] Tran, F. & Blaha, P. Accurate band gaps of semiconductors and insulators with a semilocal exchange-correlation potential. *Phys. Rev. Lett.* **102**, 226401 (2009).

Acknowledgments

This work is supported by Nature Science Foundation of China (Grant No. 11174359), by Chinese Department of Science and Technology (Grant No. 2012CB932302), and by the Strategic Priority Research Program of the Chinese Academy of Sciences (Grant No. XDB07000000). PC is grateful to Sai Gong for some technical helps.

Author contributions

BGL conceived and supervised the project, and PC carried out all the calculations. PC and BGL both contributed to the analysis and discussions of the results, and BGL and PC wrote the manuscript.

Additional information

Competing financial interests: The authors declare no competing financial interests.